Enhanced Ionic Conductivity of Layered-MnO_2 accompanied Morphology Evolution for Aqueous Zinc-Ion Battery

Mohamad Afiefudin[1] & Asep Ridwan Setiawan[1*]

[1]Faculty of Mechanical and Aerospace Engineering, Intstitut Teknologi Bandung, Bandung 40116, Indonesia
*Email: asep.ridwans@itb.ac.id

Abstract. Enhancing ionic conductivity is crucial for improving the performance of cathode materials in zinc-ion battery applications. In this study, nanoscale manipulation with nickel intercalation into the layered-MnO_2 cathode structure was achieved through a hydrothermal reaction at 160°C for 10 hours. The electrochemical evaluation of Ni-layered-MnO_2 involved measurements within an electrolyte of 2 M $ZnSO_4$ and 0.2 M $MnSO_4$. The results of Ni-layered-MnO_2 synthesis showed a distinctive peak of layered-MnO_2 cathode, as indicated by XRD results, and increased conductivity; its ionic conductivity was analyzed through electrochemical impedance spectroscopy (EIS), enabling rapid diffusion of Zn^{2+} ions and electron transfer. The distinctive morphology and structure of Ni-doped layered-MnO_2 through scanning electron microscope (SEM) contribute to enhanced ionic conductivity and facilitate ion transportation, positioning it as a promising cathode material for aqueous zinc-ion battery applications.

Keywords: *battery, ionic conductivity, morphology, ni-doped, and zinc ion.*

1 Introduction

Considerable potential has propelled rechargeable zinc-ion batteries (ZIB) to become highly competitive commercial batteries. Their intrinsic safety, abundant zinc reserves, low cost, and ideal specific capacity make them a promising solution, addressing concerns associated with lithium-ion batteries (LIB) Xu, et al. [1]. MnO_2 is a cost-effective, low-toxicity material for aqueous zinc-ion batteries with a high theoretical capacity, making it a practical choice. Nonetheless, MnO_2 suffers from low electronic conductivity (10^{-5} S/cm – 10^{-6} S/cm), which leads to unsatisfactory performance, such as low capacity and low capability Huang, et al. [2]. Various strategies have been explored to enhance the ionic conductivity of manganese-based materials. These include coating, doping reported by Gunaydin, et al. [3], heterostructure reported by Tu, et al. [4], and altering morphology and measuring temperature. Tiancheng Tu, et al. [4] successfully prepared MnO_2 by introducing phenylphosphonic acid (H_2PP) via a hydrothermal method, and the addition of 0.5% H_2PP presented high ionic conductivity and electrochemical kinetics. Gunaydin, et al. [3] noted that doping

Diterima 19 Januari 2024, Direvisi 5 Februari 2024, Diterima untuk dipublikasikan 6 Agustus 2024

ISSN:0852-6095, DOI: 10.5614/MESIN.2024.30.1.4

materials and altering measuring temperature contributed to improving ionic properties.

In this study, Ni-doped layered-MnO_2 was synthesized using a hydrothermal process. The resulting Ni-doped layered-MnO_2 and pure layered-MnO_2 were utilized as cathode-active materials to assess ionic conductivity and electrochemical behavior. Both Ni-doped layered-MnO_2 and pure layered-MnO_2 exhibited high ionic conductivity typical of the hydrothermal process. The Ni-doped layered-MnO_2 showed morphology evolution, enhanced ionic conductivity, and excellent electrochemical performance. These findings suggest the promise of Nickel-doped layered-MnO_2 in developing cathode materials of zinc ion batteries and for various electrochemical applications.

2 Experimental Section

In short, 2.37 g $KMnO_4$ (99.0% Sigma-Aldrich) and 0.363 g $Ni(NO_3)_2.6H_2O$ (98.5% Sigma-Aldrich) were dissolved in 30 ml deionized water at 60°C. The solution was vigorously stirred for 30 minutes, transferred to a 50 ml Teflon-lined autoclave, and maintained at 160°C for 10 hours. After reaching room temperature, the resulting product underwent three rounds of rinsing with deionized water and ethanol before drying at 80°C in a vacuum oven. Layered-MnO_2 was synthesized using a similar procedure, excluding the addition of $Ni(NO_3)_2.6H_2O$.

The samples were characterized by X-ray diffractometry (XRD, Bruker D8, CuKα irradiation) and scanning electron microscopy (SEM Hitachi SU3500). To evaluate ionic conductivity and electrochemical performance, the samples were fabricated to cathode by blending the samples as active material, C65, and carboxymethyl cellulose (CMC) in a weight ratio of 8:1:1. The resulting slurry was then uniformly coated onto titanium foil. The cathode's thickness, area, and mass loading were 0.5×10^{-2} – 0.6×10^{-2} cm, 2.0114 cm^2, and 1-2 $mg.cm^2$, respectively. Pure zinc foil served as an anode, and the electrolyte comprised 2 $ZnSO_4$ and 0.2 $MnSO_4$. The ionic conductivity of Ni-doped layered-MnO_2 and pure layered-MnO_2 was measured by electrochemical impedance spectroscopy (EIS, Autolab) in the frequency range from 10000 Hz to 0.001 Hz. The cyclic voltammetry and battery performances were tested using Corrtest and Neware battery systems.

3 Result and Discussion

3.1 Structure and Morphology

X-ray diffraction (XRD) analysis is conducted to gather details about a material's structure, chemical composition, and phases. Figure 1a displays the XRD patterns for Ni-layered-MnO_2 and layered-MnO_2 prepared through hydrothermal methods. The pattern of Ni-doped layered-MnO_2 and pure layered-MnO_2 (Fig. 1a) exhibit two main peaks at 12.5^o and 35.4^o the distinctive peaks indexed to the (001) and (200) planes of layered-MnO_2 (PDF 01-080-1098) following literature references Zhang, et al. [5], Xiao, et al. [6], Zhang, et al. [7], each unit comprises MnO_6 with an octahedral structure Zhu, et al. [8]. The introduction of nickel influences layered-MnO_2, evidenced by increased crystallinity, as observed in the higher intensity of the Ni-layered-MnO_2 diffraction pattern. Furthermore, the XRD pattern indicates the absence of other phases, affirming the sample's purity without impurities and alignment with the database Zhang, et al. [5], Zhang, et al. [7]. Fig. 1b and c show SEM images of Ni-doped layered-MnO_2 and pure layered-MnO_2. The morphology of pure layered-MnO_2 presents nanoparticles with a diameter of about 200-500 nm and many interconnected nanoflakes on its surface. Ni-doped layered-MnO_2 shows morphology evolution that forms nanoparticles like flowered (Fig. 1c).

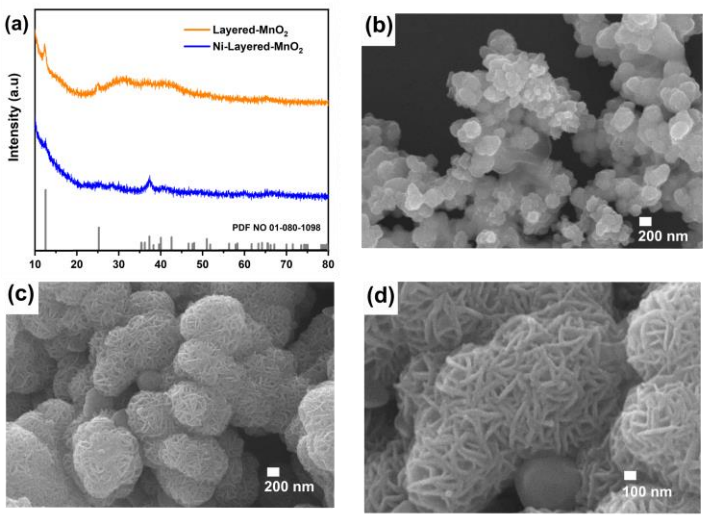

Figure. 1. (a) XRD pattern of Ni-doped layered-MnO_2 and pure layered-MnO_2, (b) SEM image of pure layered-MnO_2, (c) SEM image of pure Ni-doped layered-MnO_2, and (d) SEM image of pure Ni-doped layered-MnO_2 at higher resolution.

Scanning electron microscopy-energy dispersive spectroscopy (SEM-EDS) was used to analyze the morphology and element distribution of the hydrothermal method. The Hydrothermal treatment significantly increased crystallinity. Furthermore, The addition of Ni-layered-MnO_2 showed a higher level of crystallinity than layered-MnO_2. Increasing crystallinity in Ni-layered-MnO_2 affects changes in morphology, as seen in the SEM images (Fig. 1c and d). Element distribution mapping (Fig. 2b-d) reveals a uniform Mn, O, and Ni distribution throughout the Ni-layered-MnO_2 structure. Additionally, the SEM-EDS spectrum (Fig. 2e) indicates the presence of potassium (K), carbon (C), and silicon (Si), attributed to sample preparation during synthesis. The silicon (Si) peak is notably high, originating from the silicon wafer used as the sample pressing medium. This distribution confirms the integration of Ni into the Mn-O matrix. The Ni-layered-MnO_2 structure effectively reinforces the layered-MnO_2 structure, preventing breakdown during long cycles and enhancing electrical conductivity Zhu, et al. [8], Worku, et al. [9].

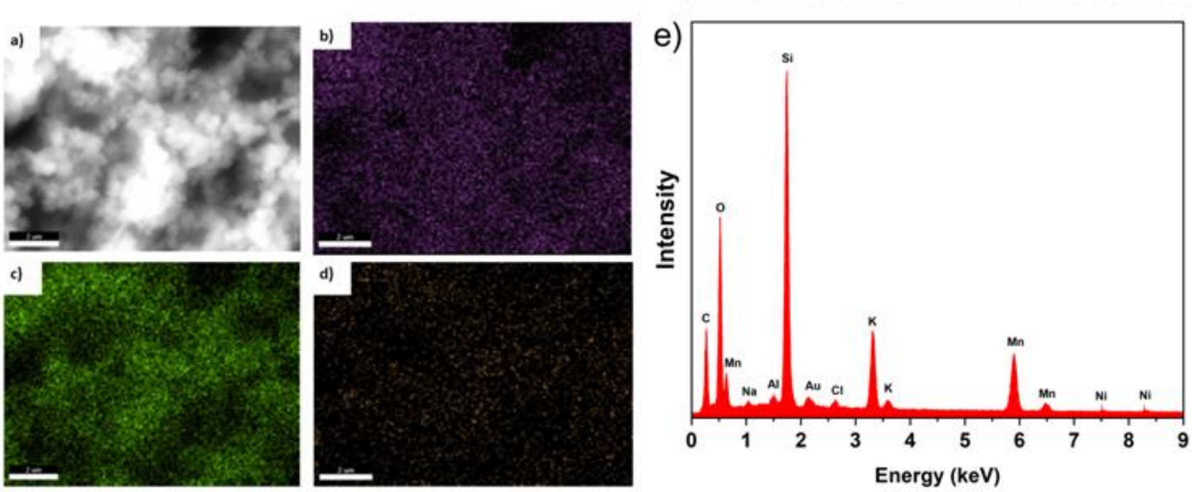

Figure 2. (a) SEM image of Ni-doped layered-MnO_2, element distribution of (b) Mn, (c) O, (d) Ni, and (e) EDS spectrum.

4 Ionic Conductivity and Electrochemical Performance

The cathode's ionic conductivity (σ) was tested by EIS and calculated using the following equation: $\sigma = L/(R_b \times A_s)$ Cai, et al. [10]. Fig. 3a and b displayed the Nyquist plot of Ni-doped layered-MnO_2 and pure layered-MnO_2; the bulk resistance was 1.3 Ω and 1.9 Ω, respectively. The corresponding ionic conductivity of Ni-doped layered-MnO_2 and pure layered-MnO_2 was 1.91×10^{-3} S/cm and 1.31×10^{-3} S/cm, respectively. It can be seen from these results that the ionic conductivity of Ni-doped layered-MnO_2 had a higher value compared to pure layered-MnO_2. Notably, pure layered-MnO_2 in this study demonstrated higher ionic conductivity than reported in the literature Huang, et al. [2]. This improvement is attributed to the enhanced ionic conductivity of nickel Patil, et al. [11].

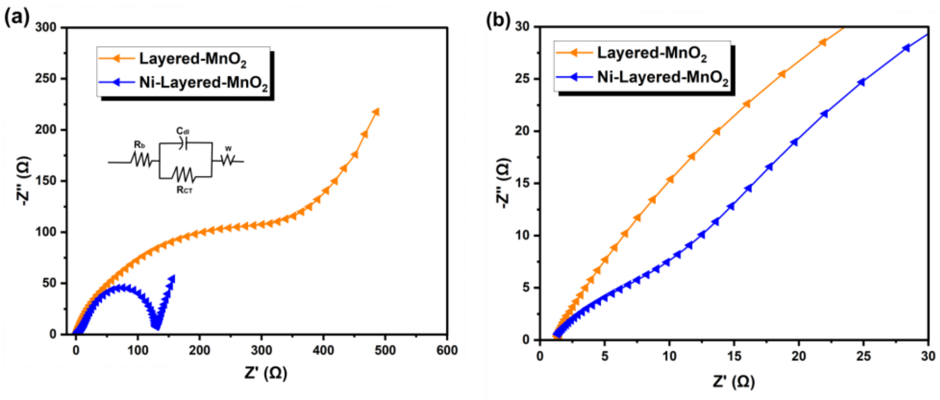

Figure. 3. (a) Nyquist plot of Ni-doped layered-MnO_2 and pure layered-MnO_2 and (b) the bulk resistance Ni-doped layered-MnO_2 and pure layered-MnO_2.

5 Electrochemical Performance

Electrochemical performance testing utilized a CR2032 coin-type battery assembled in the open air. The electrode preparation involved mixing the active material, conductive carbon, and carboxymethyl cellulose (CMC) in a weight ratio of 8:1:1, combined in deionized water. The resulting slurry was poured onto a titanium foil current collector and dried at 80°C. The electrode's mass loading (mass to electrode area) is approximately 1-2 mg/cm^2. Electrolyte solutions consisted of 2 molar $ZnSO_4$ and 0.2 molar $MnSO_4$. The anode was composed of zinc, with a Whatman sheet (GF/A) serving as a separator between the anode and cathode. Cyclic voltammetry (CV) covered a voltage range of 0.8-1.9 V at scan rates 0.2 mV.s^{-1}, and electrochemical impedance spectroscopy (EIS) spanned a frequency range from 10,000 Hz to 0.001 Hz using Corrtest and Autolab (EIS) devices. The GCD charging/discharging measurements were conducted on the Autolab Battery Tester. In Fig. 4a, the cyclic voltammetry (CV) curve for Ni-doped layered-MnO_2 exhibits two sets of redox peaks during both anodic and cathodic sweeps, indicating efficient intercalation-extraction of Zn^{2+}/H^+. The well-maintained shapes of the CV curves affirm the reversible redox reaction of the Ni-doped layered-MnO_2 cathode Wu, et al. [12], Fang, et al. [13]. The cycling performance and coulombic efficiency of Ni-doped layered-MnO_2 and pure layered-MnO_2 cathode in the voltage range of 0.8 – 1.8

V at current density 100 mA. g^{-1} are depicted in Fig. 4b. The Specific capacity calculations are based on the mass of Ni-doped layered-MnO_2 and pure layered-MnO_2 cathode. In the initial cycle, the Ni-layered-MnO_2 exhibits slightly lower capacity than layered-MnO_2 (351 mAh.g^{-1}), observed in the first 15 cycles (Fig.4b). This is attributed to H^+ and Zn^{2+} insertion reactions in the layered-MnO_2 electrode, which do not occur in the first cycle of the Ni-layered-MnO_2 electrode, where only Zn^{2+} reaction takes place Lee, et al. [14]. Additionally, the higher percentage of Mn^{2+} in layered-MnO_2 than Ni-layered-MnO_2 contributes to decreased electron storage ability. After 15 cycles, the active material on the Ni-layered-MnO_2 electrode is effectively activated, which is evident in the increased capacity (311 mAh.g^{-1}) compared to layered-MnO_2 (287 mAh.g^{-1}). In contrast, the layered-MnO_2 electrode experiences dissolution of the active material due to the John Taller effect Zhang, et al. [15]. Throughout the entire cycle, coulumbic efficiency remains at 96%. The Ni-layered-MnO_2 electrode exhibits a capacity retention of 80.4% after 50 cycles, with a capacity of 194 mAh.g^{-1}. In contrast, layered-MnO_2 experiences a significant capacity decrease, retaining only 38.7% after the 50th cycle, with a capacity of 136 mAh. g^{-1}. This disparity is attributed to the dissolution of Mn ions, leading to the breakdown of the interlayer circuit in the layered-MnO_2 structure Zhang, et al. [15]. The exceptional electrochemical performance is primarily attributed to the high ionic conductivity resulting from the intercalation of Ni^{2+} in layered-MnO_2 structure and enhanced structural stability. This structure can facilitate both ion intercalation and de-intercalation during the repeating cycle with high ion diffusion. These results promise cathode materials in zinc ion batteries and various electrochemical applications.

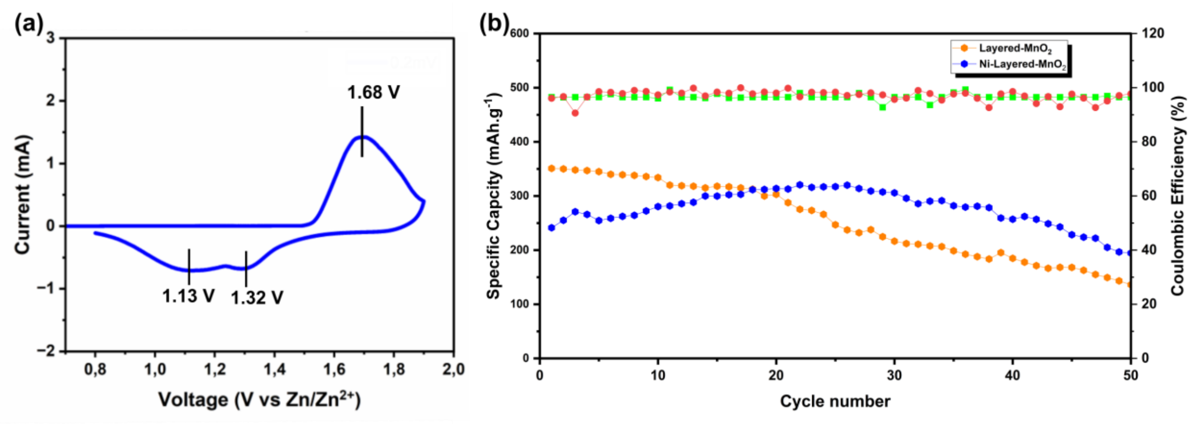

Fig. 4. (a) CV Curves at scan rates 0.2 mV.s^{-1} of Ni-doped layered-MnO_2 and (b) cycle performance at 0.1 A/g of Ni-doped layered-MnO_2 compared to layered-MnO_2.

6 Conclusion

In summary, Ni-doped layered-MnO_2 was synthesized through a simple hydrothermal process, enhancing ionic conductivity through Ni^{2+} intercalation and morphology evolution. The intercalation of Ni^{2+} at a ratio of 6:0.5 does not alter the crystal structure but substantially improves the electrochemical performance of layered-MnO_2 electrodes. This enhancement is evident in increased capacity and ion transfer speed. The Ni^{2+} intercalation in layered-MnO_2 also results in a more stable structure than pure layered-MnO_2. The Electrochemical assessments confirm that Ni^{2+} incorporation significantly enhances the material's performance by forming robust ionic bonds with oxygen atoms.

7 Acknowledgement

I thank Dr. Afriyanti Sumboja for her valuable technical assistance and insightful discussions. This study received support from the Indonesian Endowment Fund for Education (LPDP) from the Republic of Indonesia.

8 References

[1] Xu, Y., *et al.*, *Recent Advances on Challenges and Strategies of Manganese Dioxide Cathodes for Aqueous Zinc-Ion Batteries*, Energy & Environmental Materials, **6**(6), p. e12575, 2023.

[2] Huang, Y., *et al.*, *Flexible High Energy Density Zinc-Ion Batteries Enabled by Binder-Free Mno$_2$/Reduced Graphene Oxide Electrode*, npj Flexible Electronics, **2**(1), 2018.

[3] Gunaydin, S., *et al.*, *The Effect of CrFe2O4 Addition on the Ionic Conductivity Properties of Manganese-Substituted $LiFeO_2$ Material*, Journal of Electronic Materials, **53**(1), pp 367-379, 2023.

[4] Tu, T., Chen, L., & Li, L., *The Function of Phenylphosphonic Acid on Diversifying the Property of Manganese Dioxide Applied in the Aqueous Zinc-Ion Battery*, Electrochimica Acta, 2024.

[5] Zhang, X., Yu, P., Zhang, H., Zhang, D., Sun, X., & Ma, Y., *Rapid Hydrothermal Synthesis of Hierarchical Nanostructures Assembled from Ultrathin Birnessite-Type MnO_2 Nanosheets for Supercapacitor Applications*, Electrochimica Acta, **89**, pp 523-529, 2013.

[6] Xiao, W., Wang, D., & Lou, X.W., *Shape-Controlled Synthesis of MnO2 Nanostructures with Enhanced Electrocatalytic Activity for Oxygen Reduction*, The Journal of Physical Chemistry C, **114**(3), pp 1694-1700, 2010.

[7] Zhang, R., *et al.*, *Manipulating Intercalation-Extraction Mechanisms in Structurally Modulated δ-MnO_2 Nanowires for High-Performance Aqueous Zinc-Ion Batteries*, Chemical Engineering Journal, **433**, 2022.

[8] Zhu, S., Huo, W., Liu, X., & Zhang, Y., *Birnessite Based Nanostructures for Supercapacitors: Challenges, Strategies and Prospects*, Nanoscale Adv, **2**(1), pp. 37-54, 2020.

[9] Worku, A.K., Ayele, D.W., & Habtu, N.G., *Influence of Nickel Doping on MnO_2 nanoflowers as Electrocatalyst for Oxygen Reduction Reaction*, SN Applied Sciences, **3**(9), 2021.

[10] Cai, N., Wang, K., Li, N., Huang, S., & Xiao, Q., *Novel Sandwich Structured Chrysotile Fiber Separator for Advanced Lithium-Ion Batteries*, Applied Clay Science, **183**, 2019.

[11] Patil, T.S., *et al.*, *Effect of Nickel (Ni) Ion Doping on the Morphology and Supercapacitive Performance of Mn_3O_4 Thin Films*, Journal of Electronic Materials, 2023.

[12] Wu, B., *et al.*, *Graphene Scroll-Coated alpha-MnO_2 Nanowires as High-Performance Cathode Materials for Aqueous Zn-Ion Battery*, Small, **14**(13), p. e1703850, 2018.

[13] Fang, G., *et al.*, *Suppressing Manganese Dissolution in Potassium Manganate with Rich Oxygen Defects Engaged High-Energy-Density and Durable Aqueous Zinc-Ion Battery*, Advanced Functional Materials, **29**(15), 2019.

[14] Lee, B., *et al.*, *Critical Role of pH Evolution of Electrolyte in the Reaction Mechanism for Rechargeable Zinc Batteries*, ChemSusChem, **9**(20), pp. 2948-2956, 2016.

[15] Zhang, T., *et al.*, *Fundamentals and Perspectives in Developing Zinc-Ion Battery Electrolytes: a Comprehensive Review*, Energy & Environmental Science, **13** (12), pp. 4625-4665, 2020.